Preprints of the 17th IFAC Symposium on System Identification
Beijing International Convention Center
October 19-21, 2015. Beijing, China

Modeling and Identification for Pneumatic Control Valves with Stiction

Li Tang * **Lei Fang** * **Jiandong Wang** * **Qunli Shang** **

* *College of Engineering, Peking University, Beijing, China 100871*
** *College of Information Engineering, Zhejiang University of Technology, Hangzhou, China 310014*

Abstract: Stiction is a common problem in pneumatic control valves. In this work, a new semi-physical model is proposed for sticky pneumatic control valves, based on the basic components of pneumatic control valves, including valve positioner, valve actuator and valve body. The procedure of identifying parameters of the semi-physical model is presented. The semi-physical model contains some major differences with several existing data-driven models in the literature for describing the valve stiction behaviors. Experimental studies are provided to demonstrate the effectiveness of the new semi-physical model and the discrepancies of data-driven models with experimental observations.

Keywords: Pneumatic control valve, stiction, identification, semi-physical model.

1. INTRODUCTION

Industrial process plants consist of numerous control loops. The most common final control elements in the process control loops are the control valves, which manipulate fluids to compensate the negative effects of load disturbances and keep the controlled process variables close to setpoints.

Industrial surveys reported that about 20% to 30% of control loops in process industries perform poorly due to control valve nonlinearities (Bialkowski, 1993; Desborough et al., 2001). One typical control valve nonlinearity is the stiction, which has been receiving many attentions recently (Jelali and Huang, 2010). There are four challenges in the study of control valve stiction, namely, stiction modeling, detection, quantification and compensation, among which the stiction modeling is the fundamental of the other three.

The data-driven stiction models have been developed, based on the input-output analysis of sticky control valves. The Stenman model (Stenman et al., 2003) is the simplest model and is parameterized by one parameter d. Choudhury model (Choudhury et al., 2005) is the most widely used data-driven model and involves two parameters S and J. Kano model (Kano et al., 2004) can be regarded as an improved version of Choudhury model because Choudhury model is not able to deal with stochastic signals. XCH model (Xie et al., 2013) is another improved model of Choudhury model with the same merit as Kano model. He model (He et al., 2007) is very different from Choudhury model in terms of a phenomenon that the control valve stops after each movement. He model has two parameters f_s and f_d, and it is reduced to Stenman model for the special case of $f_s = d$ and $f_d = 0$. Hence, we can conclude that Kano model and He model are the two representative data-driven models for sticky control valves.

In this work, a new semi-physical model for sticky pneumatic control valves is proposed based on a thorough analysis of basic components of control valves. In particular, three signal conversion processes in the control valves are investigated carefully, namely, an electric-pneumatic conversion process in the valve positioner, a pneumatic-force conversion process in the valve actuator, and a force-position conversion process in the valve body. Compared with data-driven models, the new semi-physical model has two major differences, namely, a backlash component in the electric-pneumatic conversion process, and a dynamic part in the pneumatic-force conversion process. Owing to these major differences, the new semi-physical model is consistent with experimental data of a real control valve, while the existing data-driven models have large discrepancies with experimental observations.

The rest of the paper is organized as follows. Section 2 describes the three signal conversion processes in the control valves and proposes the new semi-physical model. Section 3 presents the procedure of identifying the parameters of the new semi-physical model. Section 4 compares the new semi-physical model with Kano model and He model. Some concluding remarks are given at Section 5.

2. MODELING THE STICKY PNEUMATIC CONTROL VALVES

In this section, we first introduce the configuration of a pneumatic control valve, then describe three signal conversion processes, and finally establish a new semi-physical model.

2.1 Configuration of a pneumatic control valve

The configuration of a typical pneumatic control valve is shown in Fig. 1. It mainly consists of three components, namely, a valve actuator, a valve body and a valve positioner. An electric control signal u is received by the positioner, which drives a nozzle-flapper mechanism shown as Fig. 2 to change the inlet air pressure p_1 of the valve

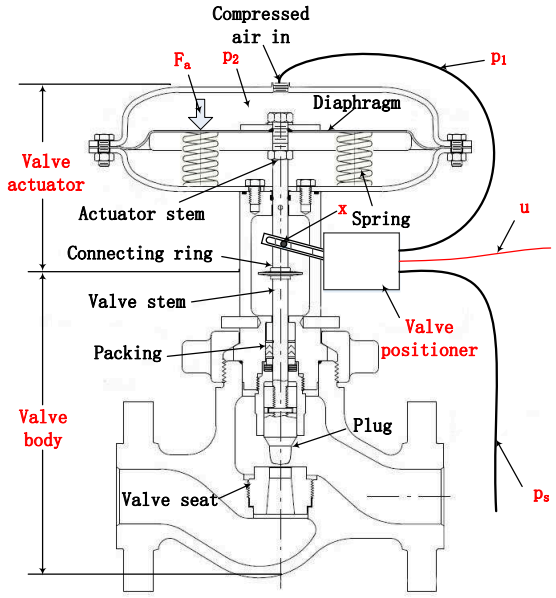

Fig. 1. Configuration of a pneumatic control valve.

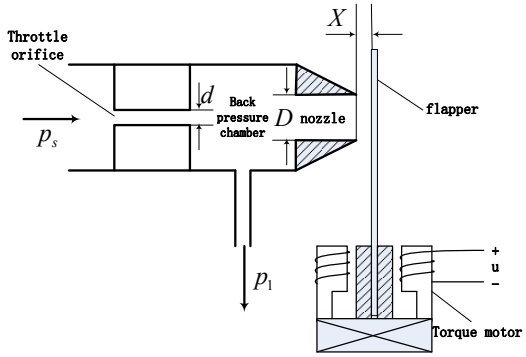

Fig. 2. A nozzle-flapper mechanism in the positioner.

actuator chamber. The air pressure p_2 inside the valve actuator chamber works on the diaphragm and forms the actuator force F_a, which overcomes the spring force and the friction forces (mainly from the tight seal between the valve stem and packing of the valve body), moves the valve stem, and determines the final valve position x.

2.2 Signal conversion processes

A model for control valves describes the relation between the electric control signal u and the valve position x. There are three signal conversion processes from u to x, namely, an electric-pneumatic conversion process from u to p_1, a pneumatic-force conversion process from p_1 to F_a, and a force-position conversion process from F_a to x. This section builds up the models for the three signal conversion processes based on physical principles involved. Note that the data-driven stiction models for control valves usually take the actuator force F_a on the diaphragm as the model inputs; thus, they only model the force-position conversion process. The transformations from the control signal u to the actuator force F_a, namely, the electric-pneumatic and pneumatic-force conversion processes, have not been considered by the data-driven stiction models to the best of our knowledge. The experimental results show that the

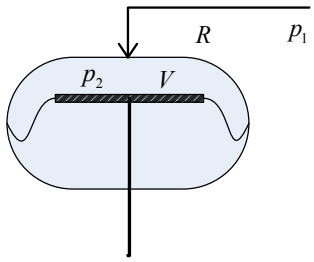

Fig. 3. Pneumatic diaphragm actuator.

transformations from u to F_a exhibit significant dynamics and nonlinearity that cannot be ignored.

Electric-pneumatic conversion process: The electric-pneumatic conversion process is achieved by the nozzle-flapper mechanism (Fig. 2) integrated in the valve positioner, which is one commonly-used electric-pneumatic convertor owing to the structural simplicity and low cost (Zhang et al., 2010). The torque motor receives the control electric signal u from a controller, and moves the flapper to vary the distance X between the nozzle and flapper, which momentarily reaches a force balance and forms p_1 as the inlet air pressure to the valve chamber. Clearly, if X is increased (decreased) by the torque motor, more (less) compressed air goes into the atmosphere through the gap between the nozzle and flapper so that p_1 is decreased (increased). Note that the transient dynamics in p_1 can be ignored when the distance X is changed by the torque motor, since the back pressure chamber has a small volume. However, a backlash nonlinearity exists in the torque motor owing to its mechanical structure, and cannot be ignored, as shown later in the experimental results in Section 4. Hence, the relation between u and p_1, with some normalization, is presented as a discrete-time backlash model,

$$p_1(t) = \begin{cases} u(t) - f_{d1}, & \text{if } \ u(t) - p_1(t-1) > f_{d1}, \\ u(t) + f_{d1}, & \text{if } \ u(t) - p_1(t-1) < -f_{d1}, \\ p_1(t-1), & \text{if } \ |u(t) - p_1(t-1)| \le f_{d1}, \end{cases} \tag{1}$$

where f_{d1} is the backlash width parameter.

Pneumatic-force conversion process: The pneumatic-force conversion process describes the dynamics from the inlet air pressure p_1 to the actuator force F_a on the diaphragm inside the valve actuator shown in Fig. 3. As $F_a = p_2 S$, where the constant S is the area of diaphragm, F_a is proportional to p_2, so that p_2 is taken as the variable in the model for the pneumatic-force conversion process. When the gas flow rate is not high, there is an approximately linear relationship between the gas flow rate and the pressure difference, namely, $Q_i = \frac{p_1 - p_2}{R}$, where Q_i represents gas flow rate and R represents air resistance. According to the ideal gas law, an equality $p_2 V = k_T N$ holds, where V is the chamber volume, N is the amount of gas in valve chamber and k_T is a constant. When the valve position x is around the operating point, the chamber volume V can be regarded as a constant. Thus, we have $Q_i = \frac{\mathrm{d}N}{\mathrm{d}t} = \frac{V \mathrm{d}p_2}{k_T \mathrm{d}t} = \frac{p_1 - p_2}{R}$. The pneumatic-force conversion process can be well approximated by a first-order linear time-invariant model,

$$F(s) = \frac{P_2(s)}{P_1(s)} = \frac{1}{\frac{RV}{k_T} s + 1}. \tag{2}$$

It is noteworthy that the mechanism of increasing and decreasing p_2 is very different: that is, when p_2 is increasing, the compressed air is injected from the air source via the nozzle-flapper structure to the valve chamber under a higher back pressure p_1 formulated by a closer distance X; when p_2 is decreasing, the compressed air in the valve chamber is discharged to the atmosphere from the gap between the nozzle and flapper. Hence, the air resistances for the injecting and discharging of the compressed air in the valve chamber, respectively denoted as R_1 and R_2, are very different. Define two time constants $T_{g1} := \frac{R_1 V}{k_T}$ and $T_{g2} := \frac{R_2 V}{k_T}$ as the ones corresponding to the injecting and discharging processes, respectively. Then, after the inverse Laplace transform of (2), the dynamics of the pneumatic-force conversion process is dependent on the direction of p_1, i.e., it can be presented as a discrete-time model

$$p_2(t) = \begin{cases} p_1(t-1) + [p_2(t-1) - p_1(t-1)] \exp(-T_s/T_{g1}), \\ \qquad \text{if } \ p_1(t) > p_2(t-1), \\ p_1(t-1) + [p_2(t-1) - p_1(t-1)] \exp(-T_s/T_{g2}), \\ \qquad \text{if } \ p_1(t) \le p_2(t-1). \end{cases} \tag{3}$$

where T_s is the sampling period, and a zero-order holder is assumed to be used between two adjacent samples of $p_1(t)$.

Force-position conversion process: The force-position conversion process converts the pneumatic actuator force F_a, or equivalently p_2, to the valve position x. A continuous-time mass-spring system has been used to describe this process (He and Wang, 2013),

$$\ddot{x} = \begin{cases} a_1(p_2 - x - f_d) - a_2\dot{x}, & \text{if } \dot{x} \ge \delta \\ a_1(p_2 - x - f_s), & \text{if } |\dot{x}| < \delta \text{ and } (p_2 - x) > f_s \\ 0, & \text{if } |\dot{x}| < \delta \text{ and } |p_2 - x| \le f_s \\ a_1(p_2 - x + f_s), & \text{if } |\dot{x}| < \delta \text{ and } (p_2 - x) < -f_s \\ a_1(p_2 - x + f_d) - a_2\dot{x}, & \text{if } \dot{x} \le -\delta \end{cases} \tag{4}$$

with properly normalized parameters as

$$a_1 = \frac{k}{m}, a_2 = \frac{F_v}{m}, f_d = \frac{F_c}{kx_m}, f_s = \frac{F_s}{kx_m}, \delta = x_m\delta_0.$$

Here k is the spring constant, m is the mass of moving parts in the valve, including the stem and plug, δ_0 is a very small constant to handle difficulties in numerical integration due to hash discontinuity caused by sign function at velocity equal to zero. F_v is the viscous friction coefficient, x_m is the valve stroke range, F_c is the Coulomb (dynamic) friction, and F_s is the static friction.

2.3 New semi-physical model

Based on the above analysis, a new semi-physical model is proposed for sticky pneumatic control valves, with the flow chart shown in Fig. 4. Here T_s is the sampling period and t is the sampling instant.

The new semi-physical model is composed of three parts. Part 1 represents the backlash nonlinearity (1) in the electric-pneumatic conversion process, where the unknown parameter is the backlash width f_{d1}. Part 2 is the direction-dependent dynamics of pneumatic-force conversion process in (3) with the unknown parameters T_{g1} and T_{g2}. Part 3 is the discrete-time counterpart of the force-position conversion process in (4), where the unknown parameters are f_s, f_d, a_1 and a_2.

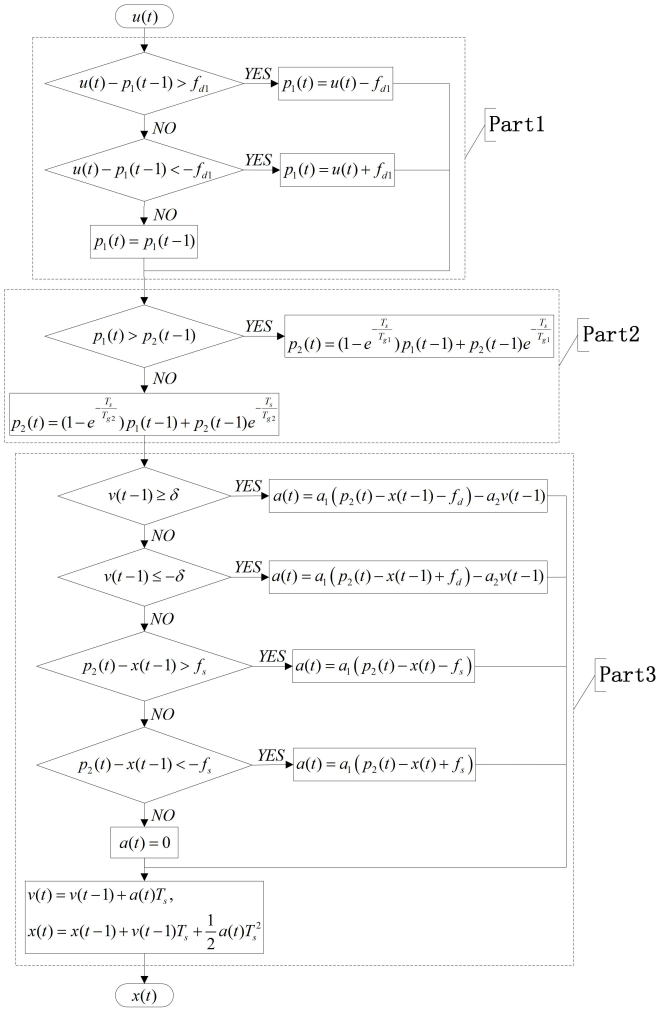

Fig. 4. Flow chart of the new semi-physical model for pneumatic control valve.

3. IDENTIFICATION OF NEW SEMI-PHYSICAL MODEL

The new semi-physical model described by (1), (3) and (4) has seven parameters to be estimated, namely, f_{d1}, T_{g1}, T_{g2}, f_d, f_s, a_1 and a_2. This section presents the experimental setup and the identification procedure for the estimation of these parameters.

3.1 Experimental setup

The experiment devices are shown in Fig. 5. The left valve is the one in experiment. The positioner receives the electric control signal u from a signal generator in Matlab® and sends the measured valve position x to the workspace of Matlab® via Instrument Control Toolbox. An air pressure sensor measures the air pressure p_2 in the valve chamber. The sampling period is 0.02 sec. Thus, the measurements of the control signal u, the chamber pressure p_2, the valve position x, and the air source pressure p_s are available in the experiment. For example, the experimental signals in a baseline test (ISA, 2006) after normalization are shown in Fig. 6.

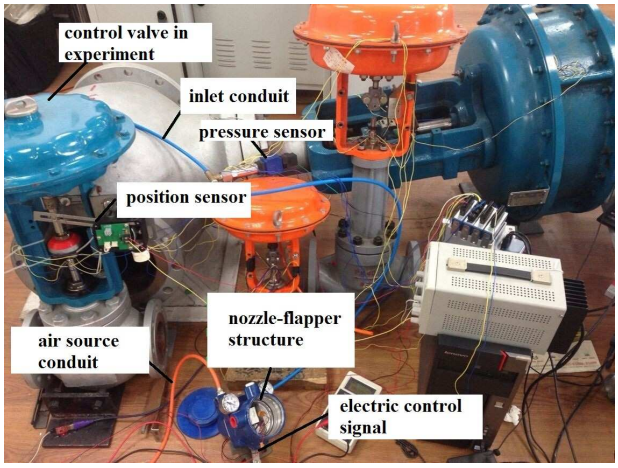

Fig. 5. Experiment devices condition

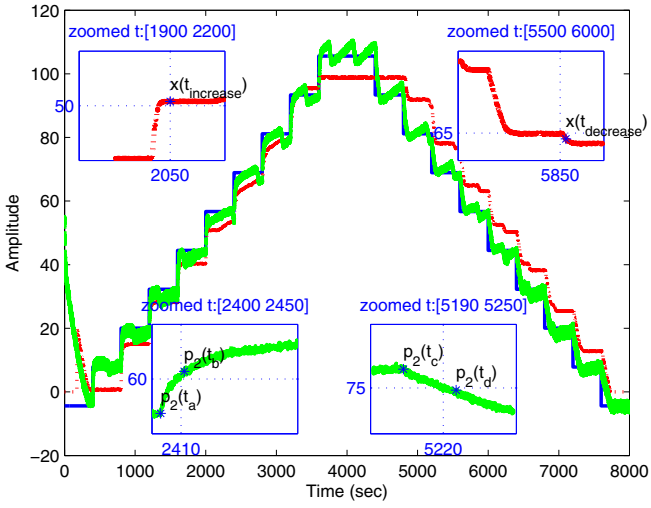

Fig. 6. The normalized control signal u (blue, solid), the normalized air pressure p_2 in valve chamber (green, dashdot) and the valve position x (red, dash) in a baseline test.

3.2 Identification of f_{d1}, f_d, T_{g1}, T_{g2} and a_1

The existence of backlash in the electric-pneumatic conversion process is revealed in an experiment shown as Fig. 7. The input u is experienced a short-time impulse at the time instant $t = 2580$ sec. In Fig. 7, the enlargement of the signal p_2 around $t = 2580$ sec shows that p_2 does not return to its original value after the impulse movement of u because of the backlash in the torque motor. The width parameter of backlash is estimated to be $\hat{f}_{d1} = \frac{1}{2}(p_2(t_{after}) - p_2(t_{before}))$, where t_{before} and t_{after} stand for the time instants when p_2 reaches its steady states before and after the impulse input, respectively. These values can be read from Fig. 7 as $t_{before} = 2540$, $t_{after} = 2619.5$, $p_2(t_{before}) = 59.7$, $p_2(t_{after}) = 62.7$; hence, $\hat{f}_{d1} = 1.5$.

The dynamic friction f_d can be estimated based on the baseline test in Fig. 6. When the control electric signal u reaches the same value from different directions, the valve positions x at steady state are different. The difference is

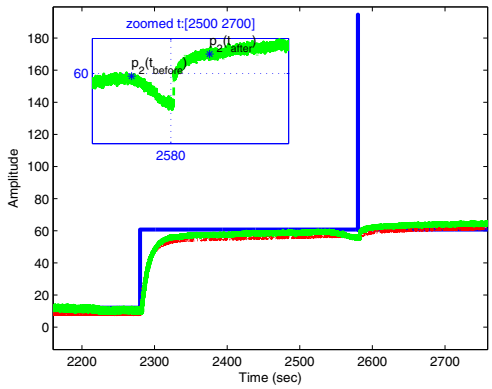

Fig. 7. Collected signals with a constant input superposed with a short-time impulse: the control signal u (blue, solid), the air pressure in valve chamber p_2 (green, dashdot) and valve position x (red, dash).

equal to the amount of dynamic friction f_d. Thus, f_d is estimated to be $\hat{f}_d = \frac{1}{2}(x(t_{decrease}) - x(t_{increase})) - \hat{f}_{d1}$, where $t_{increase}$ and $t_{decrease}$ stand for the time instants when x reaches its steady state after the increasing and decreasing step signal, respectively. These values can be read from Fig. 6 as $t_{increase} = 2050$, $t_{decrease} = 5870$, $x(t_{increase}) = 50.8$, $x(t_{decrease}) = 64.0$; hence, $\hat{f}_d = 5.1$.

The time constants T_{g1} and T_{g2} are for the increment and decrement of p_2 in the pneumatic-force conversion process, respectively. They are estimated to be $\hat{T}_{g1} = t_b - t_a$ and $\hat{T}_{g2} = t_d - t_c$. Here t_a and t_c stand for the time instances when p_2 starts to increase and decrease, respectively; t_b and t_d are the time instants when p_2 takes the value equal to 63.2% of the final values in the increasing and decreasing step responses, respectively. These values can be read from Fig. 6 as $t_a = 2403, t_b = 2411.1, t_c = 5203, t_d = 5225.5$; hence, $\hat{T}_{g1} = 8.1$ and $\hat{T}_{g2} = 22.5$.

The parameter a_1 is defined as $a_1 = \frac{k}{m} = \frac{\Delta pS}{x_m m}$. The air pressure range in the chamber is $\Delta p \approx 0.2$MPa; the area of diaphragm plate is $S \approx 0.01\text{m}^2$; the valve position range is $x_m \approx 0.1$m; the mass of moving components, including the valve stem and plug is $m \approx 10$kg. Thus, the parameter a_1 is estimated as $\hat{a}_1 = 2000$.

3.3 Identification of f_s and a_2

The parameters f_s and a_2 are determined by optimization as follows. Denote the semi-physical model shown in Fig. 4 as

$$x(t) = f(u(t); f_{d1}, T_{g1}, T_{g2}, f_d, f_s, a_1, a_2).$$

The parameters f_s and a_2 are estimated by solving the optimization problem,

$$\{\hat{f}_s, \hat{a}_s\} = \arg\min_{f_s, a_2} \frac{1}{N} \sum_{t=1}^{N} [x(t) - \hat{x}(t)]^2,$$

where

$$\hat{x}(t) = f(u(t); \hat{f}_{d1}, \hat{T}_{g1}, \hat{T}_{g2}, \hat{f}_d, f_s, \hat{a}_1, a_2).$$

Here $\hat{f}_{d1}$, $\hat{T}_{g1}$, $\hat{T}_{g2}$, $\hat{f}_d$, and $\hat{a}_1$ are the estimates in Section 3.2; N is the data length of collected samples. The estimates are $\hat{f}_s = 7$ and $\hat{a}_2 = 160$. As an illustration, the

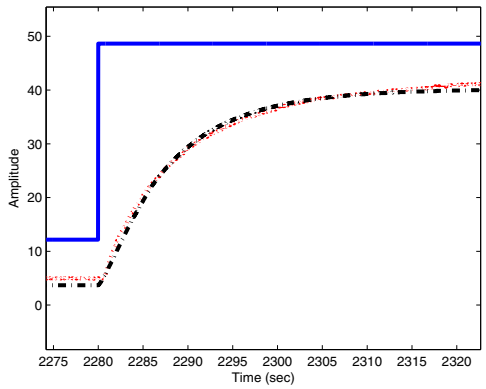

Fig. 8. The control signal u (blue, solid), measured valve position x (red, dash), and simulated valve position $\hat{x}$ (black, dashdot) for identification of f_s and a_2.

simulated valve position $\hat{x}$ is compared with $x(t)$ for a step response in Fig. 8.

4. EXPERIMENTAL STUDIES

The section compares two representative data-driven stiction models introduced in Section 1, namely, Kano model and He model, with the proposed semi-physical model in capturing the behaviors of a sticky pneumatic control valve in the experiment.

Denote He model as

$$x(t) = H(u(t); f_s, f_d),$$

where f_s and f_d stand for the static friction and dynamic friction, respectively. Similarly, define Kano model as

$$x(t) = K(u(t); S, J),$$

where S and J are the deadband plus stickband and stickband, respectively. By following the identification approach proposed in Jelali (2008), the optimal estimates of the stiction parameters f_s and f_d of He model, and the counterparts S and J of Kano model, are obtained by maximizing the fitness between x and its estimate $\hat{x}$ defined as,

$$\eta = \left(1 - \frac{||x - \hat{x}||^2}{||x - \bar{x}||^2}\right) \times 100\% \tag{5}$$

where $\bar{x}$ stands for the sample mean of x. The parameters of the proposed semi-physical model have been identified in Section 3.

4.1 Short-time impulse experiment

The control signal u is designed as a constant superposed with a short-time impulse. The measurements $\{u, x\}$ are shown in Fig. 9-(a). The stiction parameters are estimated to be $\hat{f}_s = 20.5, \hat{f}_d = 3.5$ for He model, and $\hat{S} = 24, \hat{J} = 17$ for Kano model. The simulated valve positionx $\hat{x}$ from He model, Kano model and semi-physical model are also plotted in Fig. 9. The fitnesses for He model and Kano model are the same, equal to 70.88%, while the fitness for the semi-physical model is 90.42%. More importantly, Fig. 9 says that the short-time impulse disturbance in u has little affects on the valve position x. The semi-physical model is in line with this observation; by contrast,

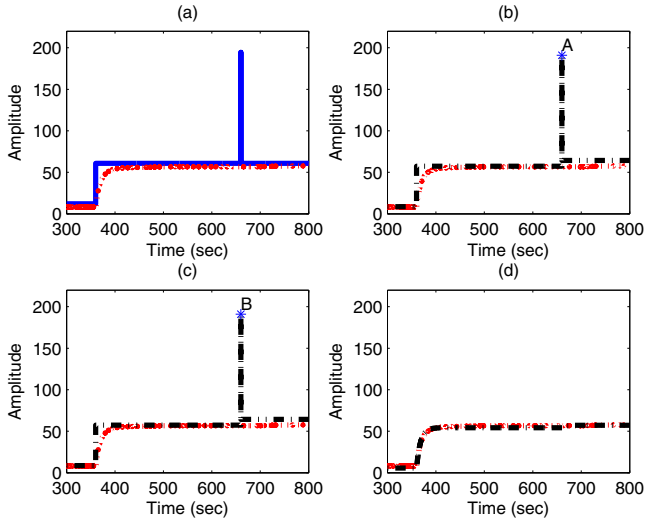

Fig. 9. Results of a short-time impulse experiment: (a) control signal u (blue, solid) and measured valve position x (red, dash); (b) x (red, dash) and $\hat{x}$ (black, dashdot) from He model; (c) x (red, dash) and $\hat{x}$ (black, dashdot) from Kano model; (d) x (red, dash) and $\hat{x}$ (black, dashdot) from the new semi-physical model.

the valve positions $\hat{x}$ from He and Kano models have large variations due to the short-time impulse, being inconsistent with the observation in the experiment.

4.2 Noisy ramp experiment

In this experiment, the control signal u is a noisy ramp signal. The collected measurements are plotted in Fig. 10-(a). The stiction parameters are estimated as $\hat{f}_s = 15.6, \hat{f}_d = 14.5$ for He model, and $\hat{S} = 30.1, \hat{J} = 1.1$ for Kano model. The fitness is $\eta = 73.76\%$ for both He and Kano models, while its counterpart for semi-physical model is $\eta = 83.49\%$. The simulated outputs $\hat{x}$ from the three models are shown in Fig. 10. The reason to repeat the identification procedure for He and Kano models instead of using the identified parameters in Section 4.1 is to achieve a better fitness performance for He and Kano models under the current measurements. Fig. 10 shows that when the input u is noisy, the measured output x is in a smooth movement; the new semi-physical model matches this observation, while He and Kano models yield sawtooth-type movements, being inconsistent with experimental results.

4.3 Closed-loop control experiment

The positioner is switched to a closed-loop control mode, subject to several reference values for desired valve positions. The reference r, controller output u and valve position x are shown in Fig. 11-(a). The stiction parameters are estimated to be $\hat{f}_s = 25.3, \hat{f}_d = 16.2$ for He model, and $\hat{S} = 40.5, \hat{J} = 8.5$ for Kano model. The fitness of He model is $\eta = 71.6\%$, and the counterpart for Kano model is $\eta = 68.81\%$, while the semi-physical model gives the fitness $\eta = 86.03\%$. The simulated valve positions are also presented in Fig. 11. In the experiment, the valve position x continuously changes. However, both two data-driven

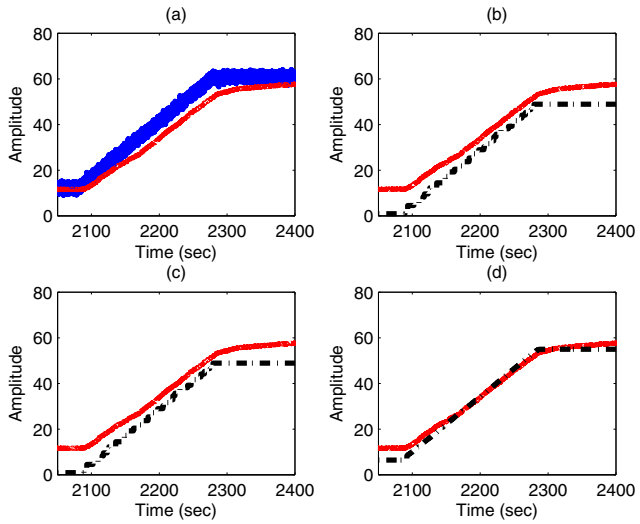

Fig. 10. Results of a noisy ramp experiment: (a) control signal u (blue, solid) and measured valve position x (red, dash); (b) x (red, dash) and $\hat{x}$ (black, dashdot) from He model; (c) x (red, dash) and $\hat{x}$ (black, dashdot) from Kano model; (d) x (red, dash) and $\hat{x}$ (black, dashdot) from the new semi-physical model.

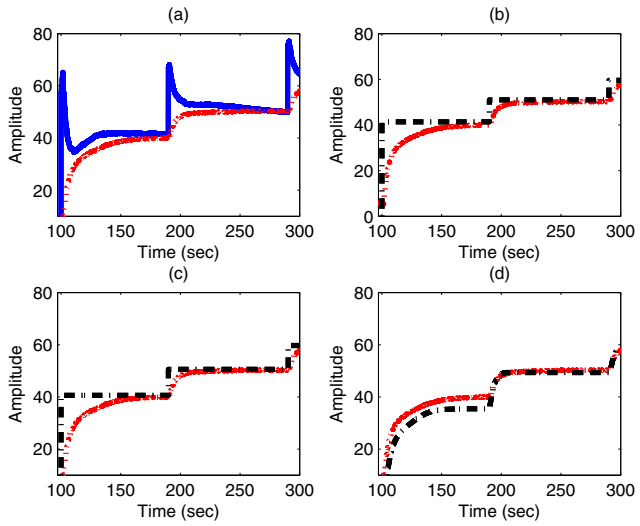

Fig. 11. Results of a closed-loop control experiment: (a) control signal u (blue, solid) and measured valve position x (red, dash); (b) x (red, dash) and $\hat{x}$ (black, dashdot) from He model; (c) x (red, dash) and $\hat{x}$ (black, dashdot) from Kano model; (d)x (red, dash) and $\hat{x}$ (black, dashdot) from the new semi-physical model.

models yield abrupt jumps, while the semi-physical model performs closely to the actual one.

The above three experiments firmly support the usage of the semi-physical model. The large discrepancies between the measured valve positions and the estimated ones of data-driven models mainly result from a fact that the models only consider the force-position conversion process, which can not fully describe the behaviors of a pneumatic control valve involving three signal conversion processes from the control signal u to the valve position x.

5. CONCLUSIONS

This paper proposed a new semi-physical model in Fig. 4 for sticky pneumatic control valves. The model is based on a careful study of three signal conversion processes, namely, the electric-pneumatic conversion process in the valve positioner, the pneumatic-force conversion process in the valve actuator, and the force-position conversion process in the valve body. Compared with data-driven models, the new semi-physical model has two major differences, namely, the backlash component in (1) for the electric-pneumatic conversion process, and the input-direction dependent dynamic part in (3) for the pneumatic-force conversion process. The differences are the fundamental reasons that the new semi-physical model behaviors consistently with experimental results of an actual control valve, while the existing data-driven stiction models have large discrepancies.

REFERENCES

Bialkowski, W.L. (1993). Dreams versus reality: a view from both sides of the gap. *Pulp and Pap. Can.*, 94, 19–27.

Choudhury, M.A.A.S., Thornhill, N.F., and Shah, S.L. (2005). Modelling valve stiction. *Control Eng. Pract.*, 13, 641–658.

Desborough, L., Nordh, P., and Miller, R. (2001). Control system reliability: process out of control. *Ind. Comput.*, 8, 52–55.

He, Q.P. and Wang, J. (2013). Quantification of valve stiction based on a semi-physical model. In *American Control Conference, 2013*, 4362–4367.

He, Q.P., Wang, J., Pottmann, M., and Qin, S.J. (2007). A curve fitting method for detecting valve stiction in oscillating control loops. *Ind. Eng. Chem. Res.*, 46(13), 4549–4560.

ISA (2006). Control valve diagnostic data acquistion and reporting. *Standard ANSI/ISA-752601-2006.*

Jelali, M. and Huang, B. (2010). *Detection and Diagnosis of Stiction in Control Loops: State of the Art and Advanced Methods.* Springer-Verlag.

Jelali, M. (2008). Estimation of valve stiction in control loops using separable least-squares and global search algorithms. *J. Process Control*, 18(7), 632–642.

Kano, M., Maruta, H., Kugemoto, H., and Shimizu, K. (2004). Practical model and detection algorithm for valve stiction. In *IFAC symposium on Dynamics and Control of Process Systems*, 5–7.

Stenman, A., Gustafsson, F., and Forsman, K. (2003). A segmentation-based method for detection of stiction in control valves. *International Journal of Adaptive control and signal processing*, 17, 625–634.

Xie, L., Cong, Y., and Horch, A. (2013). An improved valve stiction simulation model based on ISA standard tests. *Control Eng. Pract.*, 21, 1359–1368.

Zhang, X., Yin, Y., and Huang, W. (2010). Influence of temperature on null position pressure characteristics of flapper-nozzle servo valve. In *International Conference on Computer Design and Applications*, V3,257–261.